Available online at www.sciencedirect.com
SCIENCE DIRECT®
PERGAMON
International Journal of Heat and Mass Transfer 46 (2003) 4733–4739
International Journal of HEAT and MASS TRANSFER
www.elsevier.com/locate/ijhmt

Non-isothermal flow of a polymeric fluid past a submerged circular cylinder

G.H. Wu [a,*], B.Y. Wu [a], S.H. Ju [b], C.C. Wu [c]

[a] Department of Mechanical Engineering, National Cheng-Kung University, Tainan, 701, Taiwan, ROC
[b] Department of Civil Engineering, National Cheng-Kung University, Tainan, 701, Taiwan, ROC
[c] Department of Mechanical Engineering, California State University, Los Angeles, California, USA

Received 1 November 2002

Abstract

In this paper, non-isothermal flow of a polymeric liquid past a circular cylinder in an infinite domain is investigated numerically. A non-Newtonian fluid, known as a differential-type White–Metzner model, is used in the flow simulation. The computer code developed is based on the elastic-viscous split-stress finite element method incorporating the streamline-upwind Petrov–Galerkin scheme. Numerical solutions for several cases are obtained. Global flow characteristics, such as drag coefficient and heat transfer coefficient, are derived. The effects of fluid elasticity, inertia, and shear-thinning on drag and heat transfer are also investigated.

Keywords: Nusselt number; Prandtl number; Normalized drag; Polymeric fluid; Shear-thinning

1. Introduction

The non-isothermal flow of a polymeric or viscoelastic fluid past a submerged circular cylinder, as shown in Fig. 1, is considered in this study. The understanding of such a flow is required for important engineering applications and has attracted a great deal of attention in the literature. The earliest theoretical studies on this problem were conducted by Ultman and Denn [1], Mena and Caswell [2]. Decrease of drag as a quadratic function of the free stream velocity and an associated slight displacement of the streamlines downstream were concluded for small Reynolds number ($Re < 0.1$).

Experimental investigations show the effects of elasticity on the streamline patterns, drag, and heat-transfer. Manero and Mena [3] presented photographic evidence that the streamline shift may occur in either downstream or upstream, depending on the magnitude of elastic contributions to the flow. James and Acosta [4] described the measurements of heat transfer and drag for the flow of dilute polymer solutions past small cylinders, and formulated the dependence of heat-transfer and drag on fluid velocity, cylinder diameter, and polymer weights.

Numerical solutions for non-Newtonian flow around a cylinder have been established by a number of researchers. Pilate and Crochet [5] investegated a second-order fluid model at low to moderate Deborach numbers ($0 < De < 1$) and low to high Reynolds numbers ($0.1 < Re < 100$). They found that the viscoelasticity of the fluid reduces the drag at very low Reynolds numbers, while the opposite is true for high Reynolds numbers. Townsend [6] considered a shear-thinning Oldroyd model at low Deborach numbers and predicted a small displacement of the streamlines downstream, as observed experimentally by Manero. Delvaux and Crochet [7] used a mixed finite element method for a non-shear-thinning Maxwell fluid at Reynolds number ranging from 0.2 to 3.0. They found that both drag coefficient and Nusselt number depend on Reynolds number.

Recently, finite element methods have been developed to overcome the convergent difficulties encountered when simulating viscoelastic flow problems.

* Corresponding author. Tel.: +886-6-2757575x62179; fax: +886-6-2208643.
E-mail address: d1014519@mail.ncku.edu.tw (G.H. Wu).

0017-9310/$ - see front matter © 2003 Elsevier Ltd. All rights reserved.
doi:10.1016/S0017-9310(03)00018-8

Nomenclature

C_p	specific heat capacity, kJ/kg °C
De	Deborah number, dimensionless
$\boldsymbol{d}$	rate-of-deformation tensor, s^{-1}
$\boldsymbol{d}_{(1)}$	the upper-convected derivative of the rate-of-deformation tensor, s^{-2}
k	thermal conductivity, W/m K
K	normalized drag, dimensionless
Nu	Nusselt number, dimensionless
p	pressure, N/m^2
Pr	Prandtl number
Re	Reynolds number
R	radius of the cylinder, m
$\boldsymbol{s}$	the elastic part of the viscoelastic stress $\boldsymbol{\tau}$, N/m^2
We	Weissenberg number, dimensionless
U_∞	free-stream velocity, m/s
Greek symbols	
$\boldsymbol{\nabla}$	gradient operator, m^{-1}
ρ	free stream density, kg/m^3
$\boldsymbol{\tau}$	the viscoelastic stress of the polymer liquid, N/m^2
$\boldsymbol{\tau}_{(1)}$	the upper convected derivative of the viscoelastic stress $\boldsymbol{\tau}$, $N/(m^2\,s)$
$\dot{\boldsymbol{\gamma}}$	shear-rate tensor, s^{-1}
$\langle\dot{\gamma}\rangle$	average shear-rate, s^{-1}
$\eta(\dot{\gamma})$	viscosity function, Pa s
λ	relaxation-time, s
ϕ_i	quadratic basic function
ψ_i	bilinear basic function

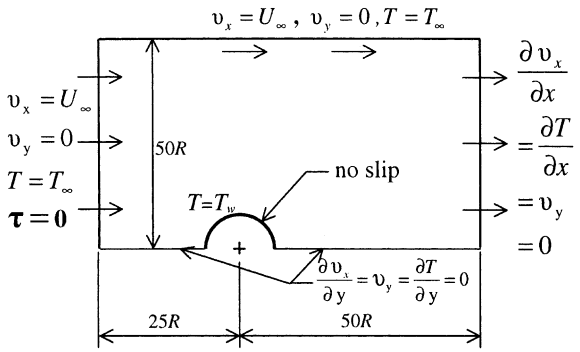

Fig. 1. Flow geometry and boundary conditions.

Marchal and Crochet [8] applied the streamline-upwind Petrov–Galerkin finite element method to discretize the constitutive equation for elastic-flow problems, each element was subdivided into a 4×4 sub-element for stress analysis, and showed good behavior for highly elastic flow problem, but was expensive in terms of computer time. Another method, called the elastic-viscous split-stress (EVSS) finite element method, was proposed by Mendelson et al. [9] in 1983 to simulate the flow of viscoelastic fluids with Newtonian viscosity such as the Oldroyd-B fluids. This method employs the splitting of the extra-stress into its viscous and elastic terms, and a change of variables for the momentum and the constitutive equations, yielding a set of equations involving the velocity $\boldsymbol{\upsilon}$, the pressure p, and the new elastic-stress $\boldsymbol{s}$. The rate-of-deformation tensor $\boldsymbol{d}$ is also introduced as an additional unknown, leading to a four-field $(\boldsymbol{\upsilon}, p, \boldsymbol{s}, \boldsymbol{d})$ problem. In 1994, the EVSS finite element method incorporating the streamline-upwind Petrov–Galerkin technique (known as the EVSS/SUPG finite element method) was proposed by Debae et al. [10] and proved to be accurate and stable for the viscoelastic flow problems with smooth boundaries.

In present study, the EVSS/SUPG finite element method is used to simulate the non-isothermal flow of polymeric fluids past a submerged circular cylinder in an infinite domain. The SUPG technique is also applied to the momentum equation to cover the high Reynolds number regimes. Consequently, the flow characteristics of the fluid are obtained. Furthermore, the effects of fluid elasticity, inertia, and shear-thinning are investigated.

2. Mathematical modelling

A viscoelastic fluid flow past a submerged circular cylinder of radius R, as shown in Fig. 1. The computational domain covers $25R$ upstream and $50R$ downstream of the cylinder. Non-isothermal flow of a viscoelastic fluid is governed by the following set of conservation and constitutive equations.

Continuity equation:

$$\boldsymbol{\nabla} \cdot \boldsymbol{\upsilon} = 0. \tag{1}$$

Momentum equation for neglecting body forces:

$$\rho(\boldsymbol{\upsilon} \cdot \boldsymbol{\nabla})\boldsymbol{\upsilon} = -\nabla p + \boldsymbol{\nabla} \cdot \boldsymbol{\tau}, \tag{2}$$

where $\boldsymbol{\tau}$ is the extra stress.

The total stress tensor is expressed as

$$\boldsymbol{\sigma} = -p\boldsymbol{I} + \boldsymbol{\tau}, \tag{3}$$

where p is pressure and $\boldsymbol{I}$ is the unit tensor.

For fluids with constant density ρ, specific heat capacity C_p, and thermal conductivity k, all being considered as constants, the energy equation for neglecting heat dissipation can be written as

$$\rho C_p \boldsymbol{\upsilon} \cdot \boldsymbol{\nabla} T = \boldsymbol{\nabla} \cdot k(\boldsymbol{\nabla} T). \tag{4}$$

The constitutive equation employs the White–Metzner type model, which was also used by Chono and Iemoto [11] to describe both the elastic and shear-thinning behavior of a 1% sodium carboxymethyl celluose (CMC) liquid as:

$$\boldsymbol{\tau} + \lambda \boldsymbol{\tau}_{(1)} = \eta \dot{\boldsymbol{\gamma}}. \tag{5}$$

The meaning of each term in Eq. (5) are summarized as follows:

Upper convective derivative of the extra stress:

$$\boldsymbol{\tau}_{(1)} = \boldsymbol{\upsilon} \cdot \boldsymbol{\nabla} \boldsymbol{\tau} - \boldsymbol{\nabla} \boldsymbol{\upsilon}^{\mathrm{T}} \cdot \boldsymbol{\tau} - \boldsymbol{\tau} \cdot \boldsymbol{\nabla} \boldsymbol{\upsilon}.$$

Shear-rate tensor:

$$\dot{\boldsymbol{\gamma}} = \boldsymbol{\nabla} \boldsymbol{\upsilon} + \boldsymbol{\nabla} \boldsymbol{\upsilon}^{\mathrm{T}}.$$

Relaxation-time function:

$$\lambda = \lambda(\dot{\gamma}).$$

Viscosity function:

$$\eta = \eta(\dot{\gamma}).$$

The relaxation-time function can be obtained via the following equation:

$$\lambda(\dot{\gamma}) = \psi_1(\dot{\gamma})/2\eta(\dot{\gamma}), \tag{6}$$

where $\psi_1(\dot{\gamma})$ is the first normal stress difference coefficient function.

The viscosity and the first normal stress difference coefficient function are defined as respectively:

$$\eta(\dot{\gamma}) = \eta_\infty + \frac{\eta_0 - \eta_\infty}{(1 + 4\lambda_1 \dot{\gamma}^2)^{(1-n)/2}}, \tag{7}$$

$$\psi_1(\dot{\gamma}) = \Psi_\infty + \frac{\Psi_0 - \Psi_\infty}{(1 + 4\lambda_2 \dot{\gamma}^2)^{(2-m)/2}}, \tag{8}$$

where η_0 and Ψ_0 are the viscosity and the primary normal stress coefficient at zero shear-rate, respectively. The parameters used in Eqs. (7) and (8) are $\eta_0 = 1.0$ Pa s, $\eta_\infty = 0.01$ Pa s, $\lambda_1 = 44.8$ s, $n = 0.608$, $\Psi_0 = 10$ Pa s^2, $\Psi_\infty = 0.001$ Pa s^2, $\lambda_2 = 10.5$ s, and $m = 0.639$.

3. Numerical method

The EVSS/SUPG finite element method has been proven to be accurate and stable for viscoelastic flow problems with smooth boundaries by Debae. The governing equations in EVSS form for the present flow problem is derived as follows.

3.1. Non-dimensional governing equations in EVSS form

In the EVSS formulation, the viscoelastic stress is split into its elastic and viscous components:

$$\boldsymbol{\tau} = \boldsymbol{s} + 2\eta \boldsymbol{d}, \tag{9}$$

where $\boldsymbol{s}$ denotes the elastic component of the viscoelastic stress and $2\eta\boldsymbol{d}$ represents the viscous component.

Upon substituting $(\boldsymbol{s} + 2\eta\boldsymbol{d})$ for $\boldsymbol{\tau}$ into Eqs. (1)–(5), the governing equations in EVSS form become:

$$\boldsymbol{\nabla} \cdot \boldsymbol{\upsilon} = 0, \tag{10}$$

$$\rho \boldsymbol{\upsilon} \cdot \boldsymbol{\nabla} \boldsymbol{\upsilon} = \boldsymbol{\nabla} \cdot (-p\boldsymbol{I} + \boldsymbol{s} + 2\eta \boldsymbol{d}), \tag{11}$$

$$\rho C_p \boldsymbol{\upsilon} \cdot \boldsymbol{\nabla} T = \boldsymbol{\nabla} \cdot k(\boldsymbol{\nabla} T), \tag{12}$$

$$\boldsymbol{s} + \lambda(\boldsymbol{s}_{(1)} + 2\eta \boldsymbol{d}_{(1)}) = 0, \tag{13}$$

$$\boldsymbol{d} - (\boldsymbol{\nabla} \boldsymbol{\upsilon} + \boldsymbol{\nabla} \boldsymbol{\upsilon}^{\mathrm{T}})/2 = 0. \tag{14}$$

When appropriate dimensionless variables are introduced, the dimensionless governing equations can be obtained as follows:

$$\boldsymbol{\nabla}^* \cdot \boldsymbol{\upsilon}^* = 0, \tag{15}$$

$$Re\ \boldsymbol{\upsilon}^* \cdot \boldsymbol{\nabla}^* \boldsymbol{\upsilon}^* = \boldsymbol{\nabla}^* \cdot (-p^* \boldsymbol{I} + \boldsymbol{s}^* + 2\eta^* \boldsymbol{d}^*), \tag{16}$$

$$Re\ Pr\ \boldsymbol{\upsilon}^* \cdot \boldsymbol{\nabla}^* T^* = \boldsymbol{\nabla}^{*2} T^*, \tag{17}$$

$$\boldsymbol{s}^* + We\ \lambda^* (\boldsymbol{s}^*_{(1)} + 2\eta^* \boldsymbol{d}^*_{(1)}) = 0, \tag{18}$$

$$\boldsymbol{d}^* - (\boldsymbol{\nabla}^* \boldsymbol{\upsilon}^* + \boldsymbol{\nabla}^* \boldsymbol{\upsilon}^{*\mathrm{T}})/2 = 0, \tag{19}$$

where the dimensionless variables are defined as follows: $x^* = x/2R$, $\boldsymbol{\upsilon}^* = \boldsymbol{\upsilon}/U_\infty$, $\nabla^* = 2R\nabla$, $\eta^* = \eta/\eta_0$, $\lambda^* = \lambda/\lambda_0$, $T^* = (T - T_\infty)/(T_w - T_\infty)$, $p^* = 2pR/(U_\infty \eta_0)$, $\boldsymbol{d}^* = 2\boldsymbol{d}R/U_\infty$, and $\boldsymbol{s}^* = 2\boldsymbol{s}R/(U_\infty \eta_0)$. The Reynolds number, Weissenberg number, and Prandtl number are defined as:

$$Re = 2\rho U_\infty R/\eta_0, \tag{20}$$

$$We = U_\infty \lambda_0 / R, \tag{21}$$

$$Pr = \eta_0 C_p / k. \tag{22}$$

3.2. Weak formulation of the non-dimensional governing equations

The field variables are interpolated within each element by

$$\boldsymbol{\upsilon}^* = \sum_{i=1}^{N=8} \phi_i \boldsymbol{\upsilon}_i^*, \quad p^* = \sum_{i=1}^{M=4} \psi_i p_i^*, \quad \boldsymbol{s}^* = \sum_{i=1}^{M=4} \psi_i \boldsymbol{s}_i^*,$$

$$\boldsymbol{d}^* = \sum_{i=1}^{M=4} \psi_i \boldsymbol{d}_i^*, \quad T^* = \sum_{i=1}^{N=8} \phi_i T_i^*,$$

where $\boldsymbol{\upsilon}_i^*$, p_i^*, $\boldsymbol{s}_i^*$, $\boldsymbol{d}_i^*$, T_i^* are nodal values and ϕ_i, ψ_i are quadratic and bi-linear basic functions, respectively.

Following the traditional Galerkin's manipulations, the weak form of the non-dimensional governing Eqs. (15) and (19) can be derived as follows:

$$\int_{\Omega} \psi_i(\nabla^* \cdot \mathbf{v}^*)\mathrm{d}\Omega = 0, \tag{23}$$

$$\int_{\Omega} \psi_i[\boldsymbol{d}^* - (\nabla^*\mathbf{v}^* + \nabla^*\mathbf{v}^{*\mathrm{T}})/2]\mathrm{d}\Omega = 0. \tag{24}$$

The traditional Galerkin method is known to be inappropriate when the convective terms in the hyperbolic constitutive equation becomes dominant as the Weissenberg number increases. The SUPG technique proposed by Brooks and Hughes [12] is therefore applied to the constitutive equation (18). An additional weighing function $(\tilde{\boldsymbol{k}}^*\mathbf{v}^*/\mathbf{v}^* \cdot \mathbf{v}^*) \cdot \nabla^*\psi_i$ is applied to all the terms of the constitutive equation. The definition of the dimensionless $\tilde{\boldsymbol{k}}^*$ can be found from [13], as originally proposed by Brooks and Hughes [12]. Hence, the following weak form is then obtained:

$$\int_{\Omega} [\psi_i + (\tilde{\boldsymbol{k}}^*\mathbf{v}^*/\mathbf{v}^* \cdot \mathbf{v}^*) \cdot \nabla^*\psi_i] \times [\boldsymbol{s}^* + We\,\lambda^*(\boldsymbol{s}^*_{(1)} + 2\eta^*\boldsymbol{d}^*_{(1)})]\mathrm{d}\Omega = 0. \tag{25}$$

Due to the relatively high Peclet and Reynolds number of this problem, the SUPG formulation developed by Brooks and Hughes is used to suppress the undesirable oscillations in the calculation of the velocity and temperature fields. To solve the two equations by this method, an additional weighing function formulation $(\tilde{\boldsymbol{k}}^*\mathbf{v}^*/\mathbf{v}^* \cdot \mathbf{v}^*) \cdot \nabla^*\phi_i$ is applied to all terms of the momentum Eq. (16) and energy Eq. (17), where $\tilde{\boldsymbol{k}}^*$ is the dimensionless form of $\tilde{\boldsymbol{k}}$ as originally proposed by Brooks and Hughes [12]. Consequently, the following weak forms are finally obtained as:

$$\int_{\Omega} [\phi_i'(Re\ \mathbf{v}^* \cdot \nabla^*\mathbf{v}^*) + \nabla^*\phi_i' \cdot (-p^*\boldsymbol{I} + \boldsymbol{s}^* + 2\boldsymbol{d}^*)\mathrm{d}\Omega] - \int_s \phi_i \boldsymbol{n} \cdot (-p^*\boldsymbol{I} + \boldsymbol{s}^* + 2\boldsymbol{d}^*)\mathrm{d}s = 0, \tag{26}$$

$$\int_{\Omega} \{\phi_i'[Re\ Pr\ \mathbf{v}^* \cdot \nabla^* T^*] + \nabla^*\phi_i' \cdot \nabla^* T^*\}\mathrm{d}\Omega - \int_s \phi_i \boldsymbol{n} \cdot \nabla^* T^*\,\mathrm{d}s = 0, \tag{27}$$

where $\phi_i' = \phi_i + (\tilde{\boldsymbol{k}}^*\mathbf{v}^*/\mathbf{v}^* \cdot \mathbf{v}^*) \cdot \nabla^*\phi_i$.

Since the integrals in Eqs. (23)–(27) are integrals of polynomial functions, they may be readily evaluated numerically by use of Gaussian quadrature. The above discretization processes lead to a system of non-linear equations of the form

$$\boldsymbol{K}(\boldsymbol{x}^*)\boldsymbol{x}^* = \boldsymbol{f}, \tag{28}$$

where $\boldsymbol{K}(\boldsymbol{x}^*)$ is global stiffness matrix, $\boldsymbol{f}$ is the force vector, $\boldsymbol{x}^* = (v_x^{*(1)} \cdots v_x^{*(n_1)},\ v_y^{*(1)} \cdots v_y^{*(n_1)},\ s_{xx}^{*(1)} \cdots s_{xx}^{*(n_2)},\ s_{yy}^{*(1)} \cdots s_{yy}^{*(n_2)},\ s_{xy}^{*(1)} \cdots s_{xy}^{*(n_2)},\ d_{xx}^{*(1)} \cdots d_{xx}^{*(n_3)},\ d_{yy}^{*(1)} \cdots d_{yy}^{*(n_3)},\ d_{xy}^{*(1)} \cdots d_{xy}^{*(n_3)},\ p^{*(1)} \cdots p^{*(n_4)},\ T^{*(1)} \cdots T^{*(n_5)}$, and n_1, n_2, n_3, n_4, n_5 are respectively the number of velocity, elastic-stress, rate-of-deformation, pressure, and temperature nodal points.

The Newton–Raphson iteration method is employed to solve the above set of non-linear equations. Due to the sparseness and asymmetry of the global stiffness matrix, the biconjugate gradient stabilized (BiCGStab) method [14] has been developed to compute all the unknowns at each iteration step. Convergence is considered to be achieved when the relative error of each of the dimensionless variables is less than 10^{-4}.

4. Results and discussion

Numerical results for the present problem have been obtained and compared for the following three types of fluids:

(1) Upper-convected Maxwell (UCM) fluid (η = constant, λ = constant),
(2) CMC fluid ($\eta = \eta(\dot{\gamma})$, $\lambda = \lambda(\dot{\gamma})$),
(3) Newtonian fluid (η = constant, $\lambda = 0$).

The CMC fluid is the shear-thinning case of the UCM fluid, and the Newtonian fluid is the simply inelastic case.

The fluid properties and the geometry are fixed, while the free streamline velocity U_∞ is allowed to vary. Simulations are performed for *Re* numbers ranging from 0.5 to 8, corresponding to Weissenberg numbers (*We*) ranging from 0.063 to 1.0. Three finite-element meshes containing 216, 436, and 896 elements (labeled M1, M2, and M3, respectively) are used for the computation domain, as shown in Fig. 2. The number of nodes and degrees of freedom (DOF) associated with each mesh are summarized in Table 1.

4.1. Drag on the cylinder

The total drag force on the cylinder is simply the sum of the stream-wise components of the normal and shear stresses, and can be easily found by the following equation due to Dhahir and Walters [15]. For unit length of the cylinder:

$$D = -2\int_0^{\pi} [\sigma_{xx}\cos\theta + \sigma_{xy}\sin\theta]_{r=R} R\,\mathrm{d}\theta, \tag{29}$$

where $\sigma_{xx} = -p + \tau_{xx}$ and $\sigma_{xy} = \tau_{xy}$.

Consequently, the drag coefficient can be obtained readily as:

$$C_{\mathrm{D}} = \frac{D}{A_{\mathrm{f}}(\rho U_\infty^2/2)}, \tag{30}$$

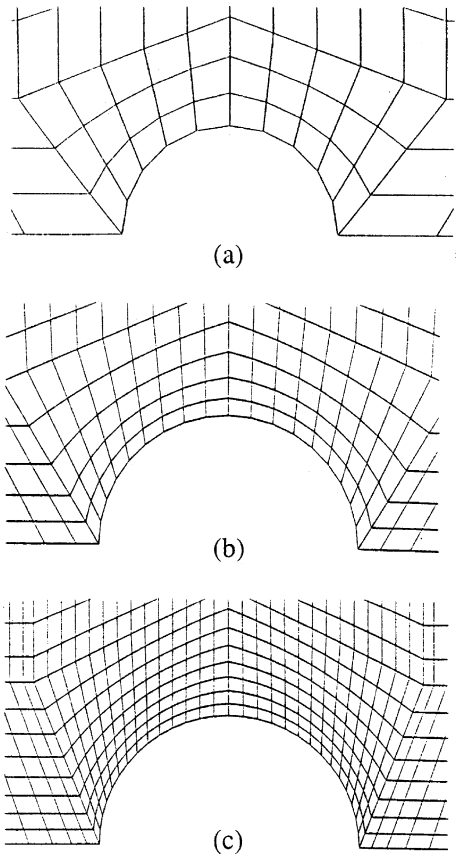

Fig. 2. Central portions of the finite element meshes used in the current simulation: (a) mesh M1; (b) mesh M2; (c) mesh M3.

Table 1
Characteristics of the finite element meshes used

MESH	No. of elements	No. of nodes	No. of DOF
M1	216	982	7812
M2	436	2086	16684
M3	896	4024	35624

where ρ = fluid density, U_∞ = free-stream velocity, and $A_f = 2\pi R$.

Numerical solutions for C_D as a function of Re are plotted in Fig. 3 for both the CMC and Newtonian fluids. The drag coefficients (C_D) is first obtained for the CMC fluid for all three meshes. Solutions of C_D from mesh M2 and mesh M3 are virtually identical, indicating that mesh M2 is sufficiently fine to obtain reasonable solutions. Hence, only mesh M2 is used for subsequent computations. To partially validate the code, C_D for the Newtonian fluid is also obtained. The numerical results were found to be in good correspondence with Schlichting's [16] experimental data for $0 < Re < 3$. Finally, it is found that C_D decrease as Re increases for the above two fluids.

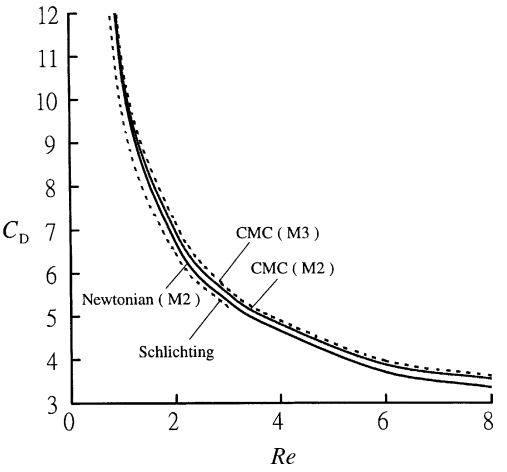

Fig. 3. C_D vs. Re for two different fluid cases.

The normalized drag K is defined as the ratio of the drag force D exerted by the viscoelastic fluid on the cylinder to its Newtonian counterpart D_N, or

$$K = D/D_N. \tag{31}$$

This ratio is plotted as a function of Reynolds number (Re) in Fig. 4 for both UCM and CMC fluids. For UCM fluid, K is found to be greater than unity and increases with Re, especially at high Re number ($Re > 6.4$), owing to the non-shear-thinning elastic effect. For CMC fluid, however, K decreases as Re increases. It can be concluded that fluid elasticity results in higher drag, while the addition of shear-thinning reduces drag.

As to investigate the effect of shear-thinning on elasticity and on viscosity separately, simulations using two additional fluid models have been performed, and the resulting C_D vs. Re for all five fluids are plotted in Fig. 5. It is clear that shear-thinning on either fluid elasticity or viscosity will decrease the drag, especially at high Reynolds number. The coupling effect of shear-thinning on both properties decreases the drag even further.

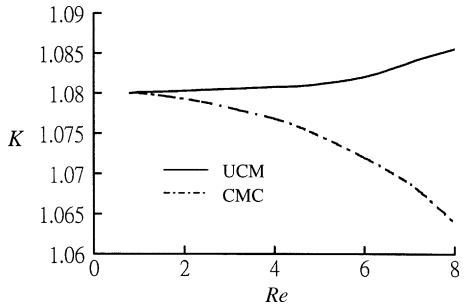

Fig. 4. Normalized drag vs. Reynolds number.

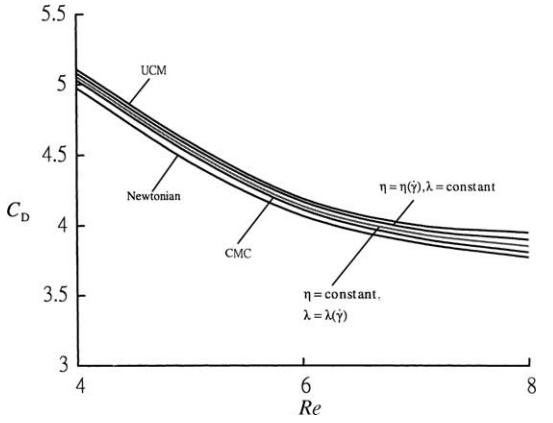

Fig. 5. C_D vs. Re for five different fluid models.

4.2. Nusselt numbers

The local Nusselt number along the cylinder wall and the overall Nusselt number are defined by the following expressions, respectively, and can be readily derived from the temperature field of numerical solutions:

$$Nu(\theta)=\left.\frac{\partial T^*}{\partial r^*}\right|_{r^*=1} \quad \text{and} \quad \overline{Nu}=\frac{1}{\pi}\int_0^{\pi} Nu(\theta)\,\mathrm{d}\theta. \tag{32}$$

The dimensionless temperature contours for three different Re are shown in Fig. 6 for CMC fluid. As the fluid flows past the heated cylinder, heat is convected downstream with the high temperature region occurring around the cylinder. Further downstream, the temperature gradually decreases as more heat is convected away. It can be seen that the high temperature region becomes smaller as Re becomes higher. Fig. 7 shows the variation of $\overline{Nu}$ with Re for all three fluids. Due to the fact that a larger amount of heat is removed from the immersed cylinder with increased Re, $\overline{Nu}$ also increases. However, for UCM fluid, it tends to approach a constant value when a critical Re is reached. This phenomenon is similar to that observed by James and Acosta [4] in their experiments on fluid modeled by the Maxwell constitutive equation. They attribute this to the stretching of the flow field because of the high Weissenberg number effect, and, as a result, reducing the velocity gradient at the cylinder surface. This phenomenon is attenuated for the shear-thinning CMC fluid, but is not found in the Newtonian case. The effects of shear-thinning on fluid elasticity and on viscosity are investigated separately, and the results are summarized in Fig. 8. It is observed that shear-thinning on either fluid

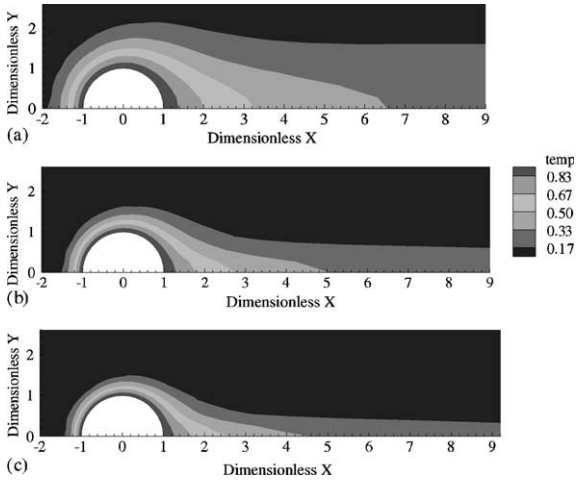

Fig. 6. Partial view of dimensionless temperature contours for three Reynolds numbers (a) $Re=1.0$, (b) $Re=4.0$ and (c) $Re=8.0$.

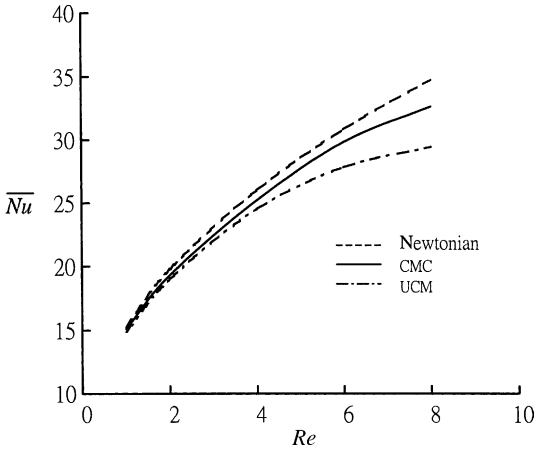

Fig. 7. $\overline{Nu}$ vs. Re for three different fluid cases.

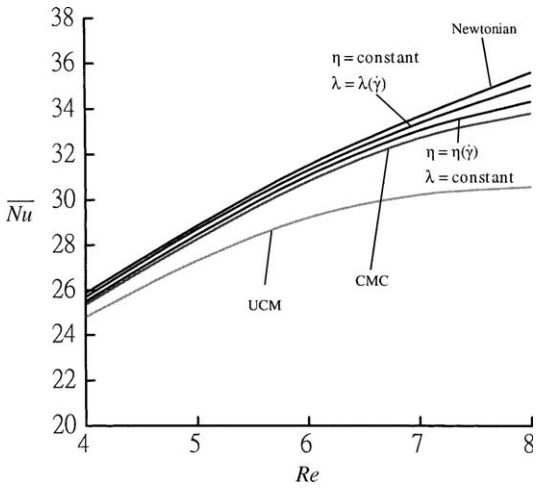

Fig. 8. $\overline{Nu}$ vs. Re for five different fluid models.

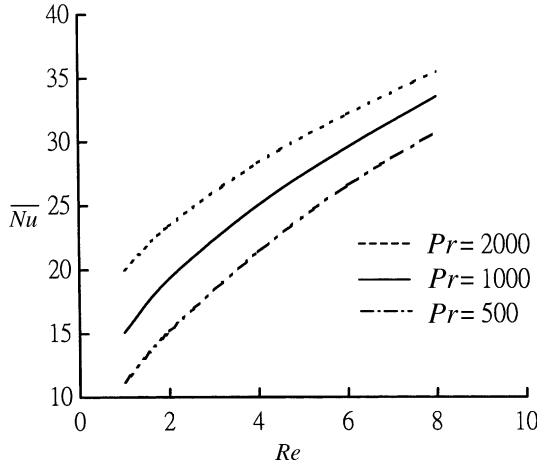

Fig. 9. $\overline{Nu}$ vs. *Re* for three values of Prandtl number.

elasticity or viscosity increases $\overline{Nu}$ with the increase of *Re*, and the coupling effect of shear-thinning on both properties further increases $\overline{Nu}$.

The effect of Prandtls number (*Pr*) is also investigated and the results are shown in Fig. 9 for the shear-thinning CMC fluid. With $Pr = 500$, 1000, and 2000, $\overline{Nu}$ is found to increase with the *Re* number. In addition, the larger Prandtls number, the larger the predicted $\overline{Nu}$. It is also observed that the variation of $\overline{Nu}$ due to different *Pr* decreases as Reynolds number increases. This is because at low *Re*, material properties has significant effect on the flow, and such effect is attenuated as inertia becomes the dominant factor at higher Reynolds number.

5. Conclusion

The EVSS/SUPG finite element method is applied to solve non-isothermal flow of a shear-thinning polymeric CMC liquid past a submerged circular cylinder. The constitutive equation adopted for this flow simulation is a differential-type White–Metzner model, which describes the non-Newtonian behavior of this fluid. The SUPG technique is used in the momentum equation to handle the high Reynolds number flow regimes. The high temperature region becomes smaller as Reynolds number becomes higher.

The effects of fluid elasticity, inertia, and shear-thinning on drag and heat transfer are investigated. It is concluded that, inertia and fluid elasticity increase drag, which can be attenuated by the addition of shear-thinning. For the three types of fluid considered, the dimensionless drag coefficient C_D decreases as Reynolds number increases, while the overall Nusselt number $\overline{Nu}$ increases with increasing Reynolds number, and approaches an asymptote for non-shear-thinning UCM fluid. The effect of Prandtls number on $\overline{Nu}$ for shear-thinning CMC fluid is found that, the larger the Prandtls number, the larger the predicted $\overline{Nu}$.

References

[1] J.S. Ultmann, M.M. Denn, Slow viscoelastic flow past submerged objects, Chem. Eng. J. 2 (1971) 81–89.
[2] B. Mena, B. Caswell, Slow flow of an elastic-viscous fluid past an immersed body, Chem. Eng. J. 8 (1974) 125–134.
[3] O. Manero, B. Mena, On the slow flow of viscoelastic liquids past a circular cylinder, J. Rheol. 32 (6) (1981) 621–639.
[4] D.F. James, A.J. Acosta, The laminar flow of dilute polymer solutions around circular cylinders, J. Fluid Mech. 42 (1970) 269–288.
[5] G. Pilate, M.J. Crochet, Plane flow of a second-order fluid past submerged boundaries, J. Rheol. 32 (6) (1981) 621–654.
[6] P. Townsend, A numerical simulation of Newtonian and viscoelastic fluid flow past stationary and rotating cylinders, Rheol. Acta 6 (1980) 219–243.
[7] V. Delvaux, M.J. Crochet, Numerical prediction of anomalous transport properties in viscoelastic flow, J. Non-Newtonian Fluid Mech. 37 (1990) 297–315.
[8] J.M. Marchal, M.J. Crochet, A new mixed finite element for calculating viscoelastic flow, J. Non-Newtonian Fluid Mech. 26 (1987) 77–114.
[9] M.A. Mendelson, P.W. Yeh, R.A. Brown, Finite element calculation of viscoelastic flow in a journal bearing: I. Small eccentricities, J. Non-Newtonian Fluid Mech. 10 (1982) 31–54.
[10] F. Debae, V. Legat, M.J. Crochet, Practical evaluation for mixed finite element methods for viscoelastic flow, J. Rheol. 38 (2) (1994) 421–442.
[11] S.S. Chono, Y. Iemoto, Numerical simulation of viscoelastic flow in two-dimensional L-shaped channels, J. Rheol. 36 (2) (1992) 335–356.
[12] N. Brooks, T.J. Hughes, Steamline upwind/Petrov–Galerkin formulation for convection dominated flows with particular emphasis on the incompressible Navier–Stokes equations, Comp. Meth. Appl. Mech. Eng. 32 (1982) 199–259.
[13] R.-Y. Chang, W.-L. Yang, Numerical simulation of non-isothermal extrudate awell at high extrusion rates, J. Non-Newtonian Fluid Mech. 51 (1993) 1–19.
[14] H.A. Van Der Vorst, BiCGSTAB: a fast and smoothly converging variant of Bi-CG for the solution of nonsymmetric linear system, SIAM J. Sci. Atat. Comput. 13 (1992) 631–644.
[15] S.A. Dhahir, K. Walters, On non-Newtonian flow past a cylinder in a confined flow, J. Rheol. 33 (1989) 781–804.
[16] H. Schlichting, Boundary Layer Theory, McGraw-Hill, New York, 1960.